Design of Magnetorheological Fluid Damper with Optimal Damping Force

Vinod Chauhan *, Ashwani Kumar, and Radhey Sham

Department of Mechanical Engineering, Chandigarh College of Engineering and Technology, Chandigarh, India
Email: vinodchauhan@ccet.ac.in (V.C.); ashwanikumar@ccet.ac.in (A.K.); radheysham@ccet.ac.in (R.S.)
*Corresponding author

***Abstract*—This article focuses on designing and analyzing of an optimal Magnetorheological Fluid Damper (MRFD) having varying piston shape channeled into the piston of the MRFD. A finite element approach has been employed to investigate the impact of piston material, piston shape, MR fluid gap and pole length on the generated magnetic field density, yield stress along with damping force. Taguchi L_{18} orthogonal array has been exercised to obtain the optimal damping force. The Analysis of Variance (ANOVA) results investigate the contribution of the selected parameters and depict that the MR fluid gap is the most predominant factor which affects the damping force, making a contribution of 77.56%, followed by piston material which contributes 12.40%, pole length with a contribution of 8.23% and piston shape has negligible contribution of 0.07%. Taguchi predicts the optimized model for the selected parameters as $A_2B_2C_1D_3$ which has been validated by carrying out the analysis using ANSYS Maxwell software v. 16. The damping force of 1053 N has been obtained for the optimal MR damper model which is based on the prediction of the Taguchi results.**

***Keywords*—Magnetorheological (MR) fluid, Finite element approach, magnetic field density, yield stress, damping force**

I. Introduction

The damping performance of Magnetorheological Fluid (MRF) damper depends upon the rheological properties of the smart working fluid. MRF contains micron-sized magnetic particles, carrier oil and suitable additives to mitigate the sedimented rate. On imposing the magnetic field, MRF transmutes from a viscous to a solid-like state and is capable to control yield stress within milliseconds. The Magnetorheological Fluid Damper (MRFD) exhibits mechanical simplicity, lesser power needs, higher dynamic range, larger force developing capability etc. Spencer *et al*. examined the capacity of the modeled dampers to estimate their responses for simple parallel plate and an axisymmetric model. Conclusively, a comparative study between the analytical and experimental results for a 20-ton Magnetorheological Fluid Damper (MRFD) damper was exhibited [1]. Parlak *et al*. [2] concentrated on optimizing the MRFD configurations by employing the Taguchi design approach. The dynamic range along with damping force was maximized by obtaining optimal solutions. Sternberg *et al*. [3] investigation focused on designing, manufacturing, and examining of a MRFD prototype. Multi-physics finite element approach was utilized to determine the coupled magnetic and fluid dynamic behaviour. Sohn *et al*. [4] proposed a novel MRFD in order to achieve an exceptional ride comfort without employing a complex controller. Sohn *et al.* [4] proposed a mathematical model of MRFD having piston bypass holes was analyzed for damping capabilities. Zhu *et al*. [5] proposed a MRFD having a compact power generating mechanism in parallel. An optimal design was given for attaining a large damping force along with a fair value of the dynamic range. Mangal and Kumar [6] designed a MRFD having optimal geometric parameters with the objective to obtain optimum value of damping force using the Taguchi technique. Hu *et al*. [7] suggested a double coiled MRFD relied on the Bingham model of MRF. A finite element approach was utilized to investigate seven varying piston configurations for optimum damping capability. The effects of the same and reversed direction of applied currents were also determined. Nie *et al*. [8] presented the design and multi-physics coupling analysis of a shear-valve-mode MRFD having various piston patterns. The impact of piston patterns in MRF gap region on Magnetic Field Density (MFD), yield stress and dynamic range was examined. Moghadam *et al.* [9] modeled a MRF damper by including the dissipative particle dynamics technique and investigated the influence of MR fluid properties on damping force. A modified Bouc-wen model was utilized as a computational strategy for validating the modelling results with experimental data.

Li and Yang [10] established a mathematical MRFD model having nonmagnetized openings within the piston which was highly effective in estimating the damping capability. The pressure drops resulting due to minor as well as viscous loss were also computed. Elsaady *et al*. [11] modeled the dynamic hysteretic behaviour in a twin-tube MRFD involving an approach that coupled the finite element analysis of the damper's magnetic circuit with computational fluid dynamics analysis. Patel *et al.* [12] made use of generalized reduced gradient and grey relation analysis optimized methodologies for modeling the shear mode MRFD for washing machine. Minitab software was

Manuscript received August 31, 2023; revised September 25, 2023; accepted October 25, 2023; published February 6, 2024.

utilized to obtain the noteworthy contributions of every selected parameter. Wei *et al*. [13] provided a systematic methodology for the optimizing the design of MRFD using a modified Bingham model so as to obtain enhanced damping capability and dynamic adjustability. In order to optimize the response parameters, a response surface method was employed. Hu *et al*. [14] evaluated the MRFD performance by making use of the multiphysics coupling simulating model which was established using the COMSOL tool. The static and dynamic magnetic field characteristics, stress distribution, and dynamic capability of the modeled damper were obtained.

Qiu *et al.* [15] observed and explored the chain structure of the MRF magnetic particles. Abdalaziz *et al*. [16] compared the MRF dampers having bypass packages and combined annular-radial fluid flow channel with the conventional MR dampers having radial fluid flow gaps. Hu *et al.* [7] set up a multi-platform joint optimized model and proposed a multi-objective optimized designing method of Design of Experiment (DOE) in combination with the surrogate model. A test system was built up and the simulation and experimentation errors for dynamic range along with the damping force were exhibited [17]. Jiang *et al.* [18] produced a unique MR damper with specified potential variables to enhance the environment adaptableness of vibrational setups provided with a particular MRF damper. Yang *et al*. [19] proposed a stepped-bypass MR damper to fulfill the damper performance need of heavy vehicles. A mathematical model was developed, and a simulation of the model was done. Jiang et al. adopted a non-dominated sorting genetic algorithm version for obtaining an optimized structure of the modeled MRFD. The structural parameters of the MRFD were found in Pareto optimized solution set obeying the minimum mass principle [20]. Ansari *et al.* [21] investigated the weight reduction along with the damping force variations by varying the MRFD annular gap and the piston configurations. The damping capability was determined at different magnitudes of MFD by varying the current in the annular gap of the modeled damper. Zare *et al*. [22] designed and obtained an optimized semi-active hybrid electromagnetic suspension setup. The performance of the designed system was evaluated on the basis of absolute regenerated power criteria, ride comfort and road holding. To enhance the vehicle's performance, a genetic algorithm was employed for the multiple-parameter optimization.

II. Modeling of Magnetorheological Fluid (MRF) Damper

The illustration of the MRFD under consideration is shown in Fig. 1. It transfers a coherent viscous damping effect for the semi active control. The most commonly employed damper is the monotube type because it is easier to install and closely packed. The piston, piston rod, and cylinder components are made up of magnetic material. A copper coil wounded over the piston generates a magnetic field when current is passed through it. The coil wires are passed through an opening in the piston rod and connected to the device controller which varies the current as per the magnitude of the vibrations. An accumulator is also included to accommodate the volume change resulting due to piston rod movement.

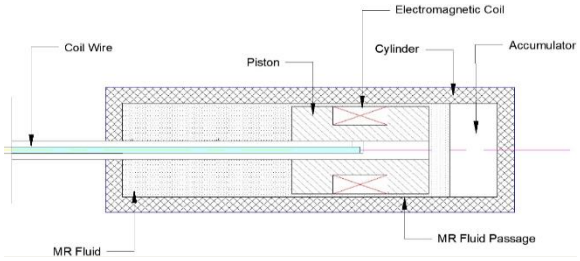

Fig. 1. Illustration of MR damper.

The MRFD is filled with MR fluids having tiny size magnetic particles dispersed into a carrier fluid. These particles constitute structured chains when made susceptible to the magnetic field and customized into semi-solid due to the viscosity enhancement. This transformation is expeditiously reversible and takes place in a few milliseconds. As the piston moves, the MR fluid passes across the MR fluid gap in-between piston and cylinder from one chamber to the another. The excited magnetic field in MR fluid gap varies the viscosity of the flowing MR fluid which in turn varies the damping force.

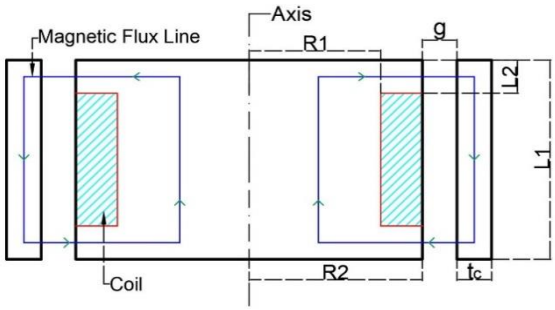

Fig. 2. Magnetic circuit for modeled MRFD.

A developed magnetic circuit for the modeled MRFD is shown in Fig. 2. The modeled MRF dampers geometrical parameters such as piston radius, internal piston radius, pole length, length of the piston head, cylinder thickness, MR fluid gap, coil width etc. are demonstrated in Table I. The 2-dimensional axi-symmetric models for all 18 MR dampers have been developed for carrying out the Finite Element Analysis (FEA). The MRF132-DG fluid parameters of the LORD company were utilized in the analysis due to the broad working temperature range of the MR fluid. The design of MRFD includes the determination of variation in generated yield stress on account of change in magnetic field density. The material selected for the piston, piston rod, and cylinder are low carbon steels (steel 1010 and steel 1008). The coil made up of copper having 360 number of turns is subjected to a current of 0.2 ampere. The equation for determining the yield stress is given in Eq. (1).

$$\tau_y = 52.962B^4 - 176.51B^3 + 158.79B^2 + 13.708B + 0.1442 \quad (1)$$

where B is magnetic field density and τ_y is yield stress.

TABLE I. THE PARAMETERS FOR MODELING 18 MRF DAMPERS

Parameter / Model No.	Piston Radius (R_1) mm	Internal Piston Radius (R_2) mm	Pole Length (L_2) mm	Cylinder Thickness (t_c) mm	Length of Piston Head (L_1) mm	Coil Width (b) mm	MR Fluid Gap (g) mm
1	13.28	24.1	8	5	45	10.82	0.9
2	11.64	24.1	10	5	45	12.46	1.1
3	9.35	24.1	12	5	45	14.75	1.3
4	15.4	24.1	8	5	45	8.70	0.9
5	14.1	24.1	10	5	45	10	1.1
6	12.3	24.1	12	5	45	11.80	1.3
7	11.73	24.1	10	5	45	12.37	0.9
8	10.39	24.1	12	5	45	13.71	1.1
9	12.81	24.1	8	5	45	11.29	1.3
10	9.35	24.1	12	5	45	14.75	0.9
11	13.28	24.1	8	5	45	10.82	1.1
12	11.64	24.1	10	5	45	12.46	1.3
13	14.1	24.1	10	5	45	10	0.9
14	12.3	24.1	12	5	45	11.80	1.1
15	15.4	24.1	8	5	45	8.70	1.3
16	10.39	24.1	12	5	45	13.71	0.9
17	12.81	24.1	8	5	45	11.29	1.1
18	11.73	24.1	10	5	45	12.37	1.3

The total generated damping force includes three components, i.e., shear force (F_τ), viscous force (F_η), and frictional force (F_f).

$$F = F_\tau + F_\eta + F_f \tag{2}$$

$$F_\eta = Q\frac{6\eta L A_p}{\pi R_{avg} g^3} \tag{3}$$

$$F_\tau = 2c\frac{L_2}{g} A_p \tau_y \operatorname{sgn}(v_p) \tag{4}$$

$$R_{avg} = R_2 + g + \frac{t_c}{2} \tag{5}$$

where Q is flowing rate, η is plastic viscosity, v_p is piston velocity, A_p is piston head cross-sectional area, R_{avg} is average radius of MR fluid gap, τ_y is yield stress and c is constant whose value ranges between 2.07–3.07, depending on the flow velocity profile. The relation used to determine this constant (c) is as follows:

$$c = 2.07 + \frac{6Q\eta}{6Q\eta + 0.4\pi R_{avg} g^2 \tau_y} \tag{6}$$

The friction force (F_f) is an undesirable component of the damping force but it can not be ignored. It is the effect of friction between various parts of the MRF damper i.e., piston seal, piston, and cylinder arrangement. In MR dampers there is a large variation of the pressure in the lower and upper region of MR damper which enhances the friction force. The friction force is a very important factor while the MR damper is in off-state. It should be very small as the lower value of friction force improves the dynamic range of the MRF dampers [23–26].

III. FINITE ELEMENT ANALYSIS OF MRF DAMPERS

Magnetostatic analysis was carried out for determining the generated magnetic field density and then relevant yield stress in the region of MR fluid for the developed damper. The various steps for the FEA process have been shown in Fig. 3.

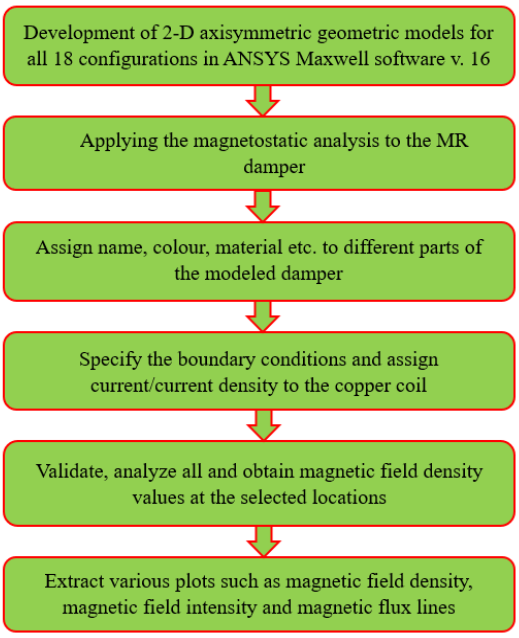

Fig. 3. Steps of Finite Element Analysis using ANSYS Maxwell software v. 16.

A. Magnetic Field Density and Yield Stress

In MRF dampers, MR fluid volume across which magnetic flux lines are passing is termed as active volume and the magnetorheological effects take place in this

region only. A higher magnetic field density in the MR fluid region makes the MRF damper more effective. In this study, it is important to assign the specific parameters as mentioned in Table II to attain the optimum geometry.

Design of experiment is a statistical methodology employed for evaluating the outcomes of multiple variables synchronically. In order to conduct experiments by Taguchi design methodology, orthogonal arrays are produced. A L_{18} Orthogonal Array (OA) shown in Table III has been chosen for obtaining various combinations of the selected factors.

TABLE II. MR DAMPER SELECTED FACTORS FOR MODELING

Parameters	Level 1	Level 2	Level 3
Piston Material (P_m)	Steel 1010	Steel 1008	–
Piston Shape (P_S)	Elliptical	Rectangular	Trapezoidal
MR Fluid Gap (g)	0.9 mm	1.1 mm	1.3 mm
Pole Length (L_2)	8 mm	10 mm	12 mm

TABLE III. SELECTED FACTORS ASSIGNED TO L_{18} OA

Model No.	Piston Material (P_m)	Piston Shape (P_S)	MR Fluid Gap (g) (mm)	Pole Length (L_2) (mm)
1	Steel 1010	Elliptical	0.9	8
2	Steel 1010	Elliptical	1.1	10
3	Steel 1010	Elliptical	1.3	12
4	Steel 1010	Rectangular	0.9	8
5	Steel 1010	Rectangular	1.1	10
6	Steel 1010	Rectangular	1.3	12
7	Steel 1010	Trapezoidal	0.9	10
8	Steel 1010	Trapezoidal	1.1	12
9	Steel 1010	Trapezoidal	1.3	8
10	Steel 1008	Elliptical	0.9	12
11	Steel 1008	Elliptical	1.1	8
12	Steel 1008	Elliptical	1.3	10
13	Steel 1008	Rectangular	0.9	10
14	Steel 1008	Rectangular	1.1	12
15	Steel 1008	Rectangular	1.3	8
16	Steel 1008	Trapezoidal	0.9	12
17	Steel 1008	Trapezoidal	1.1	8
18	Steel 1008	Trapezoidal	1.3	10

TABLE IV. MAGNETIC FIELD DENSITY AND YIELD STRESS IN MR FLUID GAP

Model No.	Magnetic Field (T)	Yield Stress (Pa)
1	0.198	7776
2	0.165	5990
3	0.135	4455
4	0.195	7595
5	0.164	5919
6	0.139	4662
7	0.183	6928
8	0.147	5067
9	0.154	5430
10	0.203	8099
11	0.207	8310
12	0.179	6732
13	0.230	9684
14	0.193	7511
15	0.182	6906
16	0.209	8452
17	0.204	8147
18	0.177	6630

The magnetic field density in the MR fluid gap region of all the 18 modeled MRF dampers have been determined using the magnetostatic tool in ANSYS Maxwell software v. 16. This software delivers solutions to amplify engineering effectiveness, simulate most complex electric/electronic design challenges and to accelerate the time of analysis [27–29]. The yield stresses (τ_y) for all the modeled dampers have been shown in Table IV. Model No.13 exhibits highest value of yield stress, while Model no. 03 exhibits the lowest value.

After determining the yield stress, shear force (F_τ) and viscous force (F_η) have been calculated using Eqs. (3–4). The value of friction force (F_f) has been fixed based on the previous literature. Then the total damping force has been calculated using Eq. (2). The major objective of the current study is to optimize the generated damping force. Table V exhibits the damping force along with S/N ratios for all 18 modeled MRF dampers.

IV. RESULTS AND DISCUSSION

The DOE approach namely Taguchi is used in the study, in which S/N ratio, the term signal corresponds to the wanted value (mean) for a response, and noise corresponds to the unwanted value, i.e., standard deviation for the response. In the current study, the attribute like damping force is the larger-the-better to improve the damping capability. The third condition given in Table VI determines the S/N ratio and its results are displayed in

Table V. The Minitab software v. 17 has been used to obtain plots for means, S/N ratios and normal probability.

TABLE V. DAMPING FORCES FOR 18 MODELED DAMPERS

Model No.	Damping Force (N)	S/N ratio
1	655.47	56.33
2	489.80	53.80
3	363.38	51.21
4	643.78	56.17
5	485.22	53.72
6	376.67	51.52
7	722.79	57.18
8	501.34	54.00
9	302.56	49.62
10	958.48	59.63
11	525.78	54.42
12	433.39	52.74
13	944.68	59.51
14	690.32	56.78
15	365.29	51.25
16	992.58	59.94
17	517.44	54.28
18	427.98	52.63

TABLE VI. SIGNAL TO NOISE (S/N) RATIO RELATIONS

Attributes	S/N ratio
Smaller is better	$-10log\left(\frac{1}{n}\sum y_i^2\right)$
Nominal is best	$-10log\left(\frac{1}{n}\sum (y_i - y_o)^2\right)$
Larger is better	$-10log\left(\frac{1}{n}\sum \frac{1}{y_i^2}\right)$

A. *Effect of Selected Parameters on Damping Force*

Figs. 4 and 5 exhibits the effect of selected parameters on damping force. It is noticed that damping force mitigates as the MR fluid gap gets widen. On the other hand, the increase in pole length enhances the damping capability of the designed damper as it allows a large number of magnetic flux lines to pass through the MR fluid region. It is also exhibited that steel 1008 generates a better damping effect as compared to steel 1010. The rectangular shaped piston of MRFD indicates a better damping capability (just marginally) in comparison to the trapezoidal and elliptical shapes.

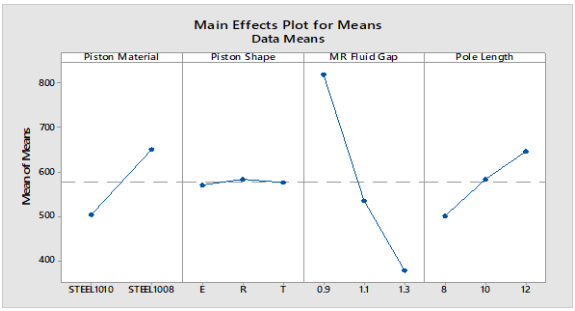

Fig. 4. Plot showing main effects for means.

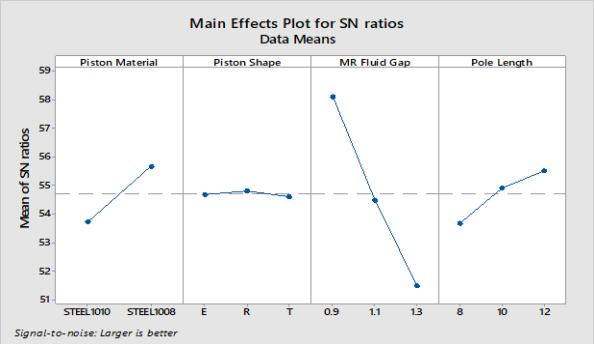

Fig. 5. Plots showing main effects for S/N ratios.

The responses of the analysis for the mean of means along with S/N ratio means of damping force are shown in Tables VII–VIII, respectively, the highest response for the damping force is observed at Level 2 for the piston material; Level 2 for the piston shape, Level 1 for the MR fluid gap and Level 3 for the pole length. Figs. 4 and 5 are the graphical demonstrations for the mean of means and the S/N ratios respectively obtained using the Taguchi design.

TABLE VII. RESPONSES FOR MEAN OF MEANS OF DAMPING FORCE (N)

Parameter / Level	Piston Material (P_m)	Piston Shape (P_S)	MR Fluid Gap (g) (mm)	Pole Length (L_2) (mm)
I	504.6	571.0	**819.6**	501.7
II	**650.7**	**584.3**	535.0	584.0
III	–	577.4	378.2	**647.1**
Delta	146.1	13.3	441.4	145.4
Rank	2	4	1	3
Mean of means of damping force = 675.4				

TABLE VIII. RESPONSES FOR MEAN OF S/N RATIOS OF DAMPING FORCE (N)

Parameter / Level	Piston Material (P_m)	Piston Shape (PS)	MR Fluid Gap (g) (mm)	Pole Length (L_2) (mm)
I	53.73	54.69	**58.13**	53.68
II	**55.69**	**54.83**	54.50	54.93
III	–	54.61	51.49	**55.51**
Delta	1.96	0.22	6.63	1.83
Rank	2	4	1	3
Mean of S/N ratios of damping force = 56.04				

B. Confirmation Test for Predicted Optimized Set of Values

In order to validate Taguchi's predicted optimized parameters combination, a conformation test is required to be carried out. The plots of magnetic field density, magnetic flux lines, and magnetic field intensity for Taguchi's predicted set of input values are shown in Figs. 6–8 respectively. Fig. 8 indicates that the MR fluid gap region has the largest values of generated magnetic field intensity.

The confirmation tests for optimized levels of selected parameters are shown in Table IX for damping force. These results exhibit an improvement in the response parameter i.e.; damping force. The S/N ratios for predicted and ANSYS Maxwell software v. 16 results are very close to each other. The S/N ratio value gets enhanced from 59.93 to 60.45. The confirmation test indicates that Taguchi predictions give better results as compared to the initially selected parameters. The damping force value gets enhanced by 6.09% when Taguchi predictions are opted.

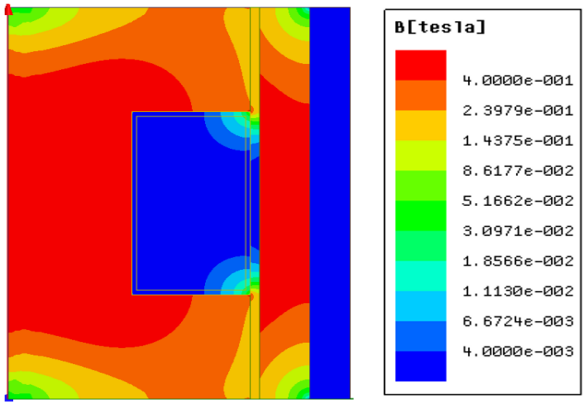

Fig. 6. Magnetic field density plot for optimized damper.

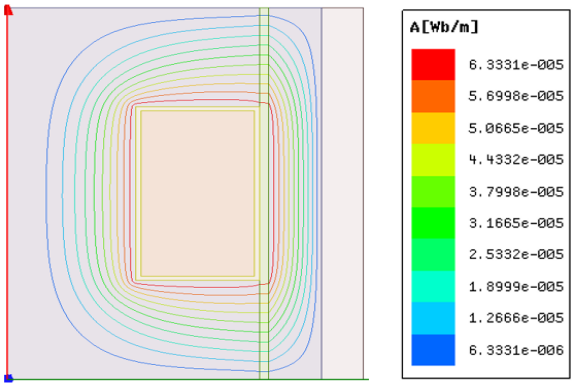

Fig. 7. Magnetic flux lines plot for optimized damper.

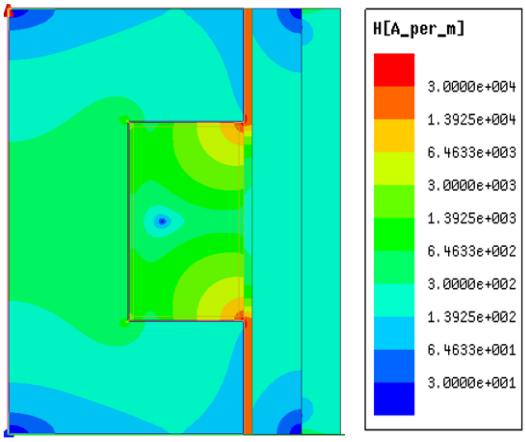

Fig. 8. Magnetic field intensity plot for optimized damper.

TABLE IX. CONFIRMATION TEST OUTCOMES FOR DAMPING FORCE

	Initial selected parameter	**Optimal process parameter**	
		Prediction	**ANSYS Maxwell software v. 16 outcomes**
Level	$A_2B_3C_1D_3$	$A_2B_2C_1D_3$	$A_2B_2C_1D_3$
Damping Force (N)	992.5	969	1053
S/N ratio	59.93%	60.03%	60.45%
Percentage improvement in damping force		**6.09%**	

Fig. 9 exhibits the variations of generated Magnetic Field Density (MFD) at the centre of the MR fluid gap varying across the length of the piston head (L_1). It shows that the MFD value in the pole length region of the MR fluid gap has a higher value, while in the MR fluid region lying between coil and cylinder, there is a sharp decline in the value of generated the MFD. It occurs because only a few numbers of flux lines are passing across this particular region.

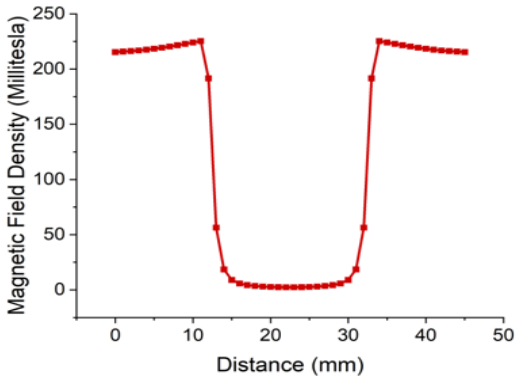

Fig. 9. Magnetic field density across MR fluid gap centre versus distance plot for optimized damper.

C. Analysis of Variance (ANOVA) for Damping Force

Analysis of Variance (ANOVA) comes up with the parameters that predominantly impact the response characteristic, i.e., damping force. The obtained results (shown in Table X) predict that the MR fluid gap (g), piston material (P_m), pole length (L_2), and piston shape (P_S) contribute 77.56%, 12.40%, 8.23% and 0.07% respectively.

The F–value for the different selected parameters has been shown in Table X. It is highest for the MR fluid gap and lowest in case of the piston shape. The coefficient of regression (R^2) is one of the most suitable methods to determine the goodness of fit for the developed model. It varies from zero to one, its closeness to one reflects a good fit. The R^2 value for the model is determined as 98.26% shown in Table X, which states its higher goodness of fit. Fig. 10 exhibits the normal probability plot and it has been noticed that the maximum number of obtained residuals lie near the straight line which signifies the good fitted developed MRFD model. The residuals signify the difference between the actual values and the fitted values suggested by the fit regression model.

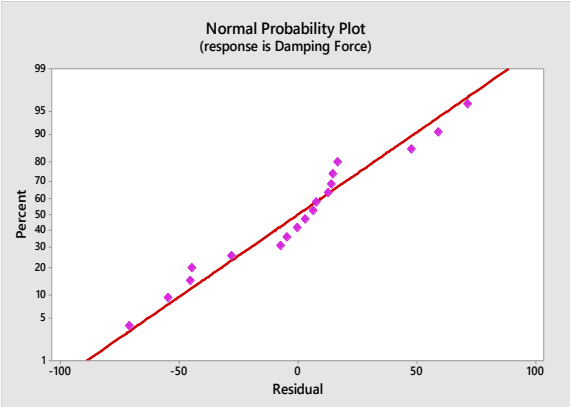

Fig. 10. Normal probability plot for residuals.

TABLE X. ANOVA RESULTS FOR THE OBTAINED DAMPING FORCE

Parameter	DF	SS	MS	F–value	Contribution
Piston Material	1	96060	96060	71.15	12.40%
Piston Shape	2	529	265	0.20	0.07%
MR Fluid Gap	2	600904	300452	222.54	77.56%
Pole Length	2	63795	31898	23.63	8.23%
Model Summary: R–square = 98.26%					
DF: degree of freedom; MS: mean square and SS: sum of square					

V. CONCLUSIONS

In the present study, MR dampers characteristics have been investigated. Eighteen damper models having different configurations, designed by Taguchi design of experiment L_{18} Orthogonal Array (OA), are modeled in solidworks and analyzed in ANSYS Maxwell software v. 16. All the modeled dampers are characterized based upon their damping force values. In conformity with the obtained results, the conclusions drawn are as follow:

- Among the 18 modeled dampers, model no. 16 exhibits the maximum value of the damping force and model no. 09 exhibits the lowest value of the damping force.
- From the optimization study, the optimal parametric combination is summed up to be $A_2B_2C_1D_3$ i.e., "second level of parameter A (piston material), second level of parameter B (piston shape), first level of parameter C (MR fluid gap) and third level of parameter D (pole length)".
- By calculating the mean of the damping force for all the levels of input parameters, the MR fluid gap has been ranked first in deciding the selected response followed by piston material, pole length, and piston shape.
- From ANOVA results of the damping force, it has been concluded that the MR fluid gap is the most predominant factor which affects the damping force with a contribution of 77.56%, followed by the piston material with a contribution of 12.40%, pole length with a contribution of 8.23% and the piston shape has negligible contribution of 0.07%.
- The predicted value of the S/N ratio for the optimized model (obtained by predicting Taguchi results) is 60.03. The predicted optimized model has been analyzed and validated. The damping force of 1053 N for the Taguchi suggested model

has been found better when compared to the 18 modeled dampers used in this study.

Conflict of Interest

The authors declare no conflict of interest.

Authors Contribution

Vinod Chauhan: conceptualization, modeling of MR damper, methodology, ANSYS Maxwell software v. 16 analysis, results and discussion, validation. Ashwani Kumar: Taguchi analysis, draft preparation, Radhey Sham: review and editing; all authors had approved the final version.

References

[1] B. F. Spencer, G. Yang, J. D. Carlson, and M. K. Sain, Smart "Dampers for seismic protection of structures: A full-scale study," in *Proc. Second World Conference on Structural Control*, 1998, vol. 1, pp. 417–426.

[2] Z. Parlak, T. Engin, and I. Şahin, "Optimal magnetorheological damper configuration using the Taguchi experimental design method," *Journal of Mechanical Design*, vol. 135, 2013.

[3] A. Sternberg, R. Zemp, and J. C. de la Llera, "Multiphysics behavior of a magneto-rheological damper and experimental validation," *Engineering Structures*, vol. 69, 2014.

[4] J. W. Sohn, J. S. Oh, and S. B. Choi, "Design and novel type of a magnetorheological damper featuring piston bypass hole," *Smart Materials and Structures*, vol. 24, 2015.

[5] X. Zhu, W. Wang, B. Yao, J. Cao, and Q. Wang, "Analytical modeling and optimal design of a MR damper with power generation," *IEEE International Conference on Advanced Intelligent Mechatronics*, pp. 1531–1536, 2015.

[6] S. K. Mangal and A. Kumar, "Geometric parameter optimization of magneto-rheological damper using design of experiment technique," *International Journal of Mechanical and Materials Engineering*, vol. 10, pp. 1–9, 2015.

[7] G. Hu, F. Liu, Z. Xie, and M. Xu, "Design, analysis, and experimental evaluation of a double coil magnetorheological fluid damper," *Shock and Vibration*, pp. 1–12, 2016.

[8] S. L. Nie, D. K. Xin, H. Ji, and F. L. Yin, "Optimization and performance analysis of magnetorheological fluid damper considering different piston configurations," *Journal of Intelligent Material Systems and Structures*, vol. 30, pp. 764–777, 2019.

[9] M. G. E. Moghadam, M. M. Shahmardan, and M. Norouzi, "Dissipative particle dynamics modeling of a mini-MR damper focus on magnetic fluid," *Journal of Molecular Liquids*, vol. 283, pp. 736–747, 2019.

[10] G. Li and Z. B. Yang, "Modelling and analysis of a magnetorheological damper with nonmagnetized passages in piston and minor losses," *Shock and Vibration*, pp. 1–12, 2020.

[11] W. Elsaady, S. O. Oyadiji, and A. Nasser, "A one-way coupled numerical magnetic field and CFD simulation of viscoplastic compressible fluids in MR dampers," *International Journal of Mechanical Sciences*, vol. 167, 2020.

[12] D. M. Patel, R. V. Upadhyay, and D. V. Bhatt, "Design and optimization of shear mode MR damper using GRG and GRA methods: Experimental validation," *Sadhana*, vol. 46, pp. 1–17, 2021.

[13] L. Wei, H. Lv, K. Yang, W. Ma, J. Wang, and W. Zhang, "A comprehensive study on the optimal design of magnetorheological dampers for improved damping capacity and dynamical adjustability," *Actuators MDPI*, vol. 10, no. 64, 2021.

[14] G. Hu, L. Wu, Y. Deng, L. Yu, and B. Luo, "Damping performance analysis of magnetorheological damper based on multiphysics coupling," *Actuators MDPI*, vol. 10, no. 176, 2021.

[15] J. Qiu, Y. Luo, Y. Li, J. Luo, Z. Su, and Y. Wang, "Research on a mechanical model of magnetorheological fluid different diameter particles," *Nanotechnology Reviews*, vol. 11, pp. 158–166, 2021.

[16] M. Abdalaziz, H. Vatandoost, R. Sedaghati, and S. Rakheja, "Development and experimental characterization of a large-capacity magnetorheological damper with annular-radial gap," *Smart Materials and Structures*, vol. 31, 2022.

[17] G. Hu, L. Wu, Y. Deng, L. Yu, and G. Li, "Optimal design and performance analysis of magnetorheological damper based on multiphysics coupling model," *Journal of Magnetism and Magnetic Materials*, vol. 558, 2022.

[18] R. Jiang, X. Rui, W. Zhu, F. Yang, Y. Zhang, and J. Gu, "Design of multi-channel bypass magnetorheological damper with three working modes," *International Journal of Mechanics and Materials in Design*, vol. 18, pp. 155–167, 2022.

[19] X. Yang, J. Zhu, Y. Song, and Y. Li, "Design and experimental research of stepped bypass magnetorheological damper," *Journal of Intelligent Material Systems and Structures*, vol. 34, 2023.

[20] M. Jiang, X. Rui, F. Yang, W. Zhu, and Y. Zhang, "Multi-objective optimization design for a magnetorheological damper," *Journal of Intelligent Material Systems and Structures*, vol. 33, pp. 33–45, 2022.

[21] M. A. Ansari, P. K. Meher, A. Bisoi, and A. Biswas, "Augmentation of damping force by modifying the geometrical shape of the MR damper," *Journal of the Brazilian Society of Mechanical Sciences and Engineering*, vol. 45, 2023.

[22] H. Zare, M. M. Jalili, and M. R. Fazel, "Multiobjective optimization for semi-active electromagnetic vehicle suspensions," *Journal of the Brazilian Society of Mechanical Sciences and Engineering*, vol. 45, 2023.

[23] O. Macháček, M. Kubík, Z. Strecker, J. Roupec, and I. Mazůrek, "Design of a frictionless magnetorheological damper with a high dynamic force range," *Advances in Mechanical Engineering*, vol. 11, 2019.

[24] T. H. Lee, C. Han, and S. B. Choi, "Design and damping force characterization of a new magnetorheological damper activated by permanent magnet flux dispersion," *Smart Materials and Structures*, vol. 2, 2017.

[25] Q. H. Nguyen, S. B. Choi, and J. K. Woo, "Optimal design of magnetorheological fluid-based dampers for front-loaded washing machines," *Journal of Mechanical Engineering Science*, vol. 228, pp. 294–306, 2014.

[26] A. Syrakos, Y. Dimakopoulos, G. C. Georgiou, and J. Tsamopoulos, "Viscoplastic flow in an extrusion damper," *Journal of Non-Newtonian Fluid Mechanics*, vol. 232, 2016.

[27] D. H. Wang and T. Wang, "Principle, design and modeling of an integrated relative displacement self-sensing magnetorheological damper based on electromagnetic induction," *Smart Materials and Structures*, vol. 18, 2009.

[28] P. Guo, J. Xie, and X. Guan, "Dynamic model of MR dampers based on a hysteretic magnetic circuit," *Shock and Vibration*, pp. 1–13, 2018.

[29] D. C. Chen and L. R. Chen, "Application of the Taguchi method for finite element analysis of a shear-type magnetorheological fluid damper," *Advances in Mechanical Engineering*, vol. 12, 2020.